Geophysical Journal International

Geophys. J. Int. (2016) **204,** 852–867 doi: 10.1093/gji/ggv487

GJI Geomagnetism, rock magnetism and palaeomagnetism

Inverse modelling of the reversely magnetized, shallow plumbing system hosting oil reservoirs of the Auca Mahuida volcano (Payeina retroarc, Neuquén Basin, Argentina)

John Paine,[1] Riccardo De Ritis,[2] Guido Ventura,[2,3] Mariana Longo,[4,5] Dhananjay Ravat,[6] Fabio Speranza[2] and Massimo Chiappini[2]

[1] *Scientific Computing and Application, 23 Porter Street, Parkside, Adelaide, SA* 5063, *Australia*
[2] *Istituto Nazionale di Geofisica e Vulcanologia, Via di Vigna Murata* 605, *I*-00147 *Roma, Italy. E-mail: riccardo.deritis@ingv.it*
[3] *Istituto Ambiente Marino Costiero, Consiglio Nazionale delle Ricerche, Calata Porta di Massa, interno Porto di Napoli* 80, *I*-80133 *Napoli, Italy*
[4] *YPF S.A., Macacha Güemes* 515, *Buenos Aires, Argentina*
[5] *Universidad Nacional de La Plata, Facultad de Ciencias Astronómicas y Geofísicas, La Plata, Argentina*
[6] *Department of Earth and Environmental Sciences, University of Kentucky,* 101 *Slone Research Building, Lexington, KY* 40506-0053, *USA*

Accepted 2015 November 6. Received 2015 October 30; in original form 2015 June 24

SUMMARY

The Auca Mahuida volcano (2.03–0.88 Ma) located east of the Andean thrust front in the Neuquén basin (Argentina) hosts an oil system of thermogenic origin and is affected by the NW–SE striking-faults. Intrusive bodies and the underlying Jurassic sediments constitute the reservoir rocks. Aeromagnetic data collected in the Auca Mahuida area detected multiple dipolar magnetic anomalies, many of which have reverse polarity. Palaeomagnetic measurements on rock samples collected in the field together with available age determinations indicate that the reversely magnetized sources were mainly emplaced during the Matuyama reverse polarity chron while the normal polarity sources were emplaced during the Olduvai and/or Jaramillo subchrons. The location and geometry of the intrusive bodies is poorly known and the customary magnetic inversion is rendered difficult because of multiple natural remanent magnetization directions. To address these difficulties, a voxel inversion was applied to model the vector residual magnetic intensity (VRMI) transformation of the observed total magnetic intensity data. The modelling showed a 1.5 km deep, subcircular ring-shaped intrusion below the summit of the volcano and a series of NW–SE elongated, fault-controlled intrusive bodies to depths up to 3–4 km. Our results show that magnetic data and VRMI modelling help resolve the geometry of the shallow plumbing system of volcanoes with remanently magnetized sources, and estimate the depth and geometry of potential oil reservoirs in volcanic areas.

Key words: Inverse theory; Magnetic anomalies: modelling and interpretation; Gas and hydrate systems; Backarc basin processes; Physics of magma and magma bodies; South America.

1 INTRODUCTION

Geophysical surveys using potential field methods have been widely applied to the study of volcanoes and hydrothermal systems in different tectonic settings with the aim of determining the geometry of plumbing systems, faults, and alteration zones (Barberi *et al.* 1994; Rollin *et al.* 2000; Finn *et al.* 2001; Caratori Tontini *et al.* 2010; De Ritis *et al.* 2010). Aeromagnetic surveys have been recently improved because of higher resolution acquisition and positioning systems and improvements in data processing and modelling (Portniaguine & Zhdanov 2002; Phillips 2004; Li *et al.* 2010).

In volcanic settings, aeromagnetic data are useful for detecting buried reservoirs, dike or circular conduits, hydrothermally altered rock volumes, volcano-tectonic collapses and the Curie isotherm depth (Rollin *et al.* 2000; Finn *et al.* 2001; Blanco-Montenegro *et al.* 2006; De Ritis *et al.* 2007, 2013; Nicolosi *et al.* 2014). This is particularly valuable when other geophysical methods are ineffective, for example seismic data that are difficult to collect in rough topography and often have a low signal-to-noise ratio; gravity data that are of limited use because the source bodies are small or dispersed and rocks have small density contrasts.

The Plio-Pleistocene Auca Mahuida volcano (hereafter referred to simply as Auca) lies in the Neuquén Basin (Argentina), a triangle-shaped basin located in the North Patagonia foreland region about 100 km east of the present-day Andean thrust front that includes the Agrio Fold and Thrust belt (Fig. 1a; Zapata & Folguera 2005; Ramos

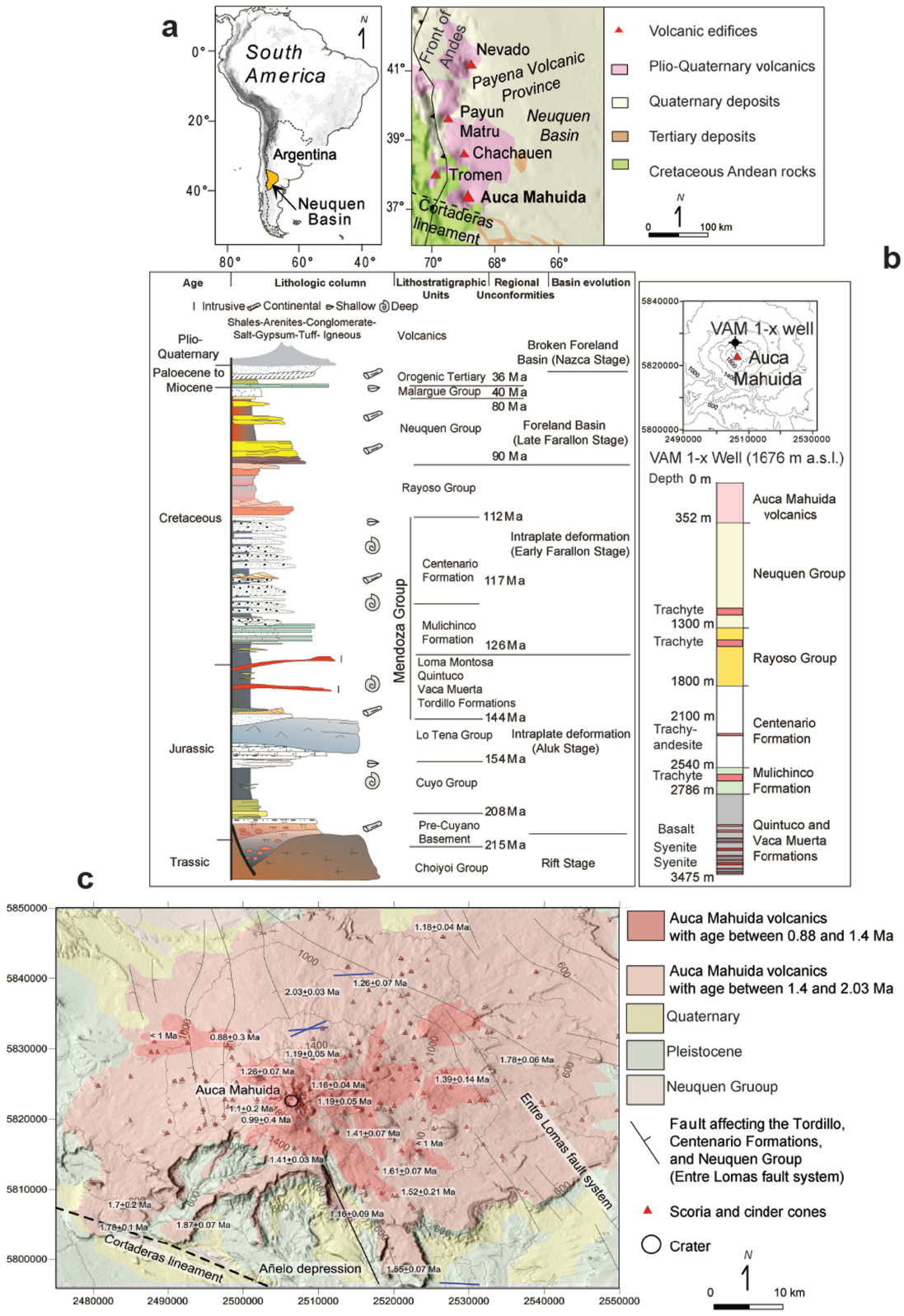

Figure 1. (a) location of the Neuquen Basin and geological sketch map of the Payena Volcanic Province (modified from Ventura *et al.* 2012). (b) Left-hand side: composite stratigraphy of the Neuquen Basin and main stages of the basin evolution (modified from Cristallini *et al.* 2006). Right-hand-side: location and stratigraphy of the VAM 1-x Well (YPF unpublished data). (c) Geological scheme of the Auca volcanic complex in UTM coordinates (WGS84 Zone 19, data from Ventura *et al.* 2012, Cristallini *et al.* 2006; Ramos & Folguera 2010). Blue thick segments indicate the location and orientation of the maximum horizontal stress (data from Guzman *et al.* 2007).

& Kay 2006). The Neuquén Basin hosts one of the most important oil fields of South America and the intrabasin Plio-Quaternary magmatism has played a key role in the formation and accumulation of the oil, which has a prevailing thermogenic origin in the Auca sector (Rossello *et al.* 2002). The Neuquén Basin reservoirs are part of an atypical oil system characterized by sedimentary source rocks with significant inorganic H_2S that were exposed to a wide range of temperatures due to repeated intrusions, and reservoir rocks consisting of igneous bodies fractured during cooling by thermal contraction (Rodriguez Monreal *et al.* 2009; Alberdi-Genolet *et al.* 2013). Recently, Liu *et al.* (2012) have elaborated the relation between volcanism, hydrocarbon bearing capacity and trapping processes within sedimentary basins. Specifically, rocks formed by volcanic processes lying close to the conduits show a higher porosity and permeability relative to the surrounding host rocks due to an increased number of fractures. Therefore, they could be suitable to host hydrocarbons and become oil traps detectable by the susceptibility contrast with the surrounding non-magnetic sedimentary sequence. In this context, Auca volcano is a meaningful case study because the interpretation of magnetic sources can furnish useful information about the position and geometry of intrusions affecting the petroleum system, the role of pre-existing faults in formation of laccoliths or sills (i.e. petroleum traps), and also their role in hydrocarbon generation and maturation by thermal effects. In the last decade, the Neuquén Basin area has been extensively investigated geophysically and geologically (Cristallini *et al.* 2006; Mazzarini *et al.* 2008; Messager *et al.* 2010; Ramos & Folguera 2010; Ventura *et al.* 2012). A high resolution aeromagnetic survey was carried out in 2001 by YPF S.A. oil company to obtain information about the oil/gas system hosted in the buried volcanic and sedimentary units of the Auca central sector. In the framework of anagreement between the Istituto Nazionale di Geofisica e Vulcanologia of Rome (INGV, Italy) and YPF S.A., the magnetic anomaly field interpretation of this survey is presented here, along with a novel modelling strategy appropriate for handling both induced and remanent magnetic sources.

We illustrate the inverse modelling results of the Auca magnetic anomaly field and surrounding sectors using the vector residual magnetic intensity (VRMI) transformation. We also present palaeomagnetic laboratory determinations and on-site susceptibility measurements. The purpose of this study is to investigate the shallower, inner structure of the Auca volcano, which is characterized by a complex, magnetic anomaly field mainly resulting from reversely magnetized sources. The results are considered in the context of the structural and volcanic setting that constrains the geometry of the shallow feeding system of the volcano and its relationships with pre-existing tectonic structures and potential hydrocarbon traps. We show that magnetic data can be successfully used to resolve the geometry of the plumbing system of this volcano that was emplaced mainly during a reverse chron.

2 GEOLOGICAL BACKGROUND

Auca is the southernmost volcano of the Payenia retroarc volcanic province (Fig. 1a), which extends between 35° and 38°S latitudes and lies to the east of the Andean thrust front (Ramos & Kay 2006). The Payenia retroarc developed in the last 3 Ma in response to extensional tectonics related to the rollback steepening of the slab (Ramos & Folguera 2010; Gudnason *et al.* 2012). Considering an eastward, 25°–30° dipping slab, crustal thickness of about 40 km, and the distance from the trench of about 450–500 km, the Payenia retroarc is located above the mantle wedge (Ramos & Folguera 2010). The eastern sector of Auca hosts the NW–SE striking, 'Entre Lomas' normal fault system (Fig. 1c), and the southern sector is affected by the 'Cortaderas' Lineament, a major WNW–ESE striking crustal discontinuity marking the southern boundary of the Miocene subduction (Kay *et al.* 2006).

Close to the southern border of the plateau, the Auca central volcano rises to 2253 m above the sea level (a.s.l.) at the summit crater. Geophysical data (Khazaradze & Klotz 2003; Guzman *et al.* 2007; Guzman & Cristallini 2009) and structural investigations on the Payenia retroarc (Fig. 1a; Mazzarini *et al.* 2008) highlight an active E–W striking compression. Geomorphological and neotectonic data in the Auca area (Ventura *et al.* 2012) and in the central and southern Neuquén Basin (Messager *et al.* 2010) are consistent with this direction of compression, which is related to the Plio-Quaternary eastward propagation of the Andean front in the foreland (Fig. 1a; Guzman & Cristallini 2009; Messager *et al.* 2010).

The age of Auca's erupted products is between 2.03 ± 0.3 and 0.88 ± 0.3 Ma and the rock composition varies from within-plate basalts (WPB) to trachytes (Kay & Ramos 2006; Ramos & Folguera 2010). Auca mainly consists of a pile of lava flows with a maximum thickness of about 500 m at the summit crater, below which there are sedimentary formations that are discussed below. The thickness of this lava pile decreases to virtually zero at the plateau's borders, that is at distances varying from 12 to 45 km from the crater. The Auca volcanic plateau covers approximately 75 × 62 km^2 and includes about one hundred cinder and scoria cones. The cones are concentrated in the summit area and on the eastern and western flanks of the volcano and are aligned along prevailing E–W striking fissures.

The Auca sedimentary substrata include the Mesozoic Vaca Muerta, Centenario, Rayoso and Neuquén main groups which, together with Tertiary sediments, represent the formations of the Neuquén Basin (Fig. 1b). The crystalline basement beneath the basin lies at a depth of about 5 km (Zapata & Folguera 2005). This basement is affected by N–S to NW–SE striking faults, whereas the overlying sedimentary successions form an antiform-like structure with a NW–SE striking axis. From the magnetic point of view, the local stratigraphy can be subdivided in three main units: a magnetic basement (Lower Palaeozoic-Upper Triassic volcanics, plutonic and metamorphic rocks); a non-magnetic Neuquén sedimentary sequence (Triassic to Lower Tertiary clastic, carbonatic and evaporite rocks); and a Plio-Pleistocene magnetic volcanic plateau and intrusive rocks. Radiometric dating of intrusions shows that the study area experienced three main magmatic cycles dating roughly to: 25–20 Ma (Oligocene–Lower Miocene, part of the Auca substratum belong to this phase), 15–10 Ma (Middle Miocene) and 5 Ma (Upper Miocene–Lower Pleistocene). The petrogenetic model for the study area (Kay *et al.* 2013 and references therein) indicates that the magma originated in the asthenosphere rising up to the base of the continental crust, where deep magma chambers formed. Subsequently, magma rose to shallower depths (6–10 km) below the Auca area, differentiating into more evolved products. These magmas reached the surface and erupted forming the present-day volcanic edifice. Some of the magmas rose up directly from the magma chambers at the base of the crust and penetrated the crust in the form of gabbroic intrusions and erupted basaltic lava flows. Cores and cuttings in the Auca area indicate that below the plateau the intrusive bodies are in the form of syenitic and gabbroic sills as suggested, for example, in the VAM-1-x well stratigraphy of Fig. 1(b). The geochemical signature of these bodies is consistent with that of the Auca volcanic rocks, which suggests that the

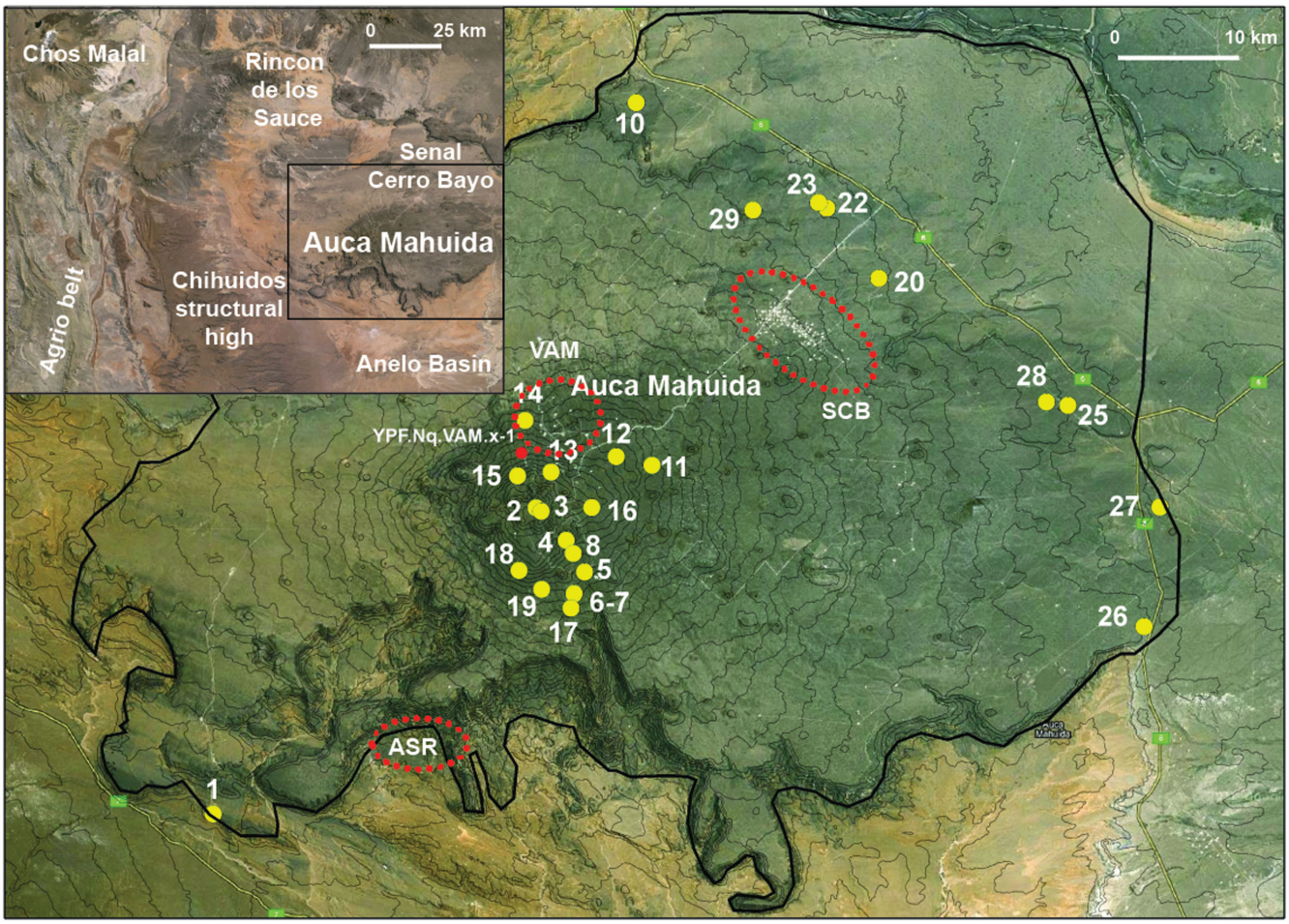

Figure 2. Satellite image of the Auca volcano (from Google Earth) with 50 m spaced contour lines. Yellow dots indicate the sample sites with numbers (white) where onsite susceptibility determination and the laboratory palaeomagnetic measurements were carried out. The red point indicates the YPF.Nq.VAM.x-1 position (see also Fig. 1b). The red dotted ellipsis indicate the position of the presently known oil field (VAM, ASR and SCB are YPF oil company acronyms). The thicker black line indicates the volcanic plateau limit. The inset shows the larger scale setting of the Auca region with the locations cited in the text and the study area (black box).

intrusions represent the crystallized portion of shallow magmatic reservoirs (Bermudez & Delpino 1998). The deeper and thicker sills intrude the Vaca Muerta Formation, which consists of shales with a total organic carbon content of 2–6 wt. per cent. These shales represent the source rocks of the petroleum system, while the overlying sandstones and fractured igneous sills are the oil reservoirs (Rossello *et al.* 2002).

3 DATA

3.1 Magnetic susceptibility and palaeomagnetic measurements

Thirty-three surface samples were collected in the field for palaeomagnetic measurements (Fig. 2). These samples are representative of the most voluminous, and extended lava flows of the Auca plateau, the volcano flanks and the summit cone. Representative samples of the sedimentary units of the upper Neuquén formation were also collected. We sampled the massive (vesicles <5 vol. per cent) portion of 25 lava flows of basaltic to trachytic composition, and measured their on-site susceptibility using a high sensitivity (1×10^{-7} SI) ZH - SM-30 magnetic susceptibility meter. The local dip and strike of each outcrop were measured and reported on the sample. The errors are in the order of 15°, which, for the qualitative evaluation of our sampling, is acceptable.

Some of the samples were cut using a microdrill and collected orthogonal to the dip and strike. The obtained cores were analysed in the laboratory of palaeomagnetism at Istituto Nazionale di Geofisica e Vulcanologia (INGV, Rome, Italy) to determine the bulk susceptibility and the natural remanent magnetization (Table 1 and Fig. 2). Magnetic susceptibility was measured with the laboratory Kappabridge system AGICO (KLY-2 model) on 30 samples; 86 per cent of the samples were from lava flows and the remainder were scoria and pumice as well as siltstones and clays of the outcropping Neuquén formation.

The natural remanent magnetization of the lava flow specimens (cut into 2 cm edge cubes) were measured in a magnetically shielded room with a DC-SQUID cryogenic magnetometer (2G Enterprises, USA), and its stability was checked by alternating field (AF) cleaning treatment up to a maximum field of 70 mT. Demagnetization data were plotted on orthogonal demagnetization diagrams (Zijderveld 1967) and the magnetization components were isolated by principal component analysis (Kirschvink 1980). The NRM from all samples was well above the noise level of the magnetometer (approximately 5×10^{-6} A m^{-1}) and generally in the 1–10 A m^{-1} range. Most of the samples could be efficiently AF cleaned at 70 mT. A viscous

Table 1. Summary of the laboratory and field rock magnetic properties measurements.

Sample	Jr (A m^{-1})	*I* (Jr)	*D* (Jr)	*k* laboratory	*k* onsite measurements sensitivity 1×10^{-7} SI	Lithology	Polarity
AM1	1.2	–29.9	333.22	0.00514	0.008371	Massive lava	N
AM2	30–40	–18.77	267.11	0.02316	0.0136556	Vesicular altered lava	N
AM3 a	15	42.05	251.68	0.00346	0.02815	Massive lava	R
AM3 b	–			–	0.02365	Massive lava	–
AM4	23	–50.51	327.16	0.03302	0.01648	Massive lava	N
AM5	35	37.92	199.06	0.04029	0.0250692	Massive lava	R
AM6	0.1			0.03839	0.01802	Massive lava\	–
AM7	2×10^{-3}			0.00506	–	Pumice	–
AM8	25	75.49	165.1	0.01283	0.009115	Massive lava	R
AM9	2	68.18	149.79	0.00667	0.005794	Vesicular lava close to a sedimentary dikes	R
AM10	3×10^{-3}			0.00023	0.0000875	Oxidized clay, volcaniclastic flow deposit	–
AM11	7	77.25	76.53	0.01834	0.0116567	Vesicular lava	R
AM12	7	–50.53	274.77	0.02631	0.0139977	Massive lava	N
AM13	3	35.2	149.88	0.02432	0.0193293	Massive lava	R
AM14	57	–17.32	360	0.01637	0.013135	Massive lava	N
AM15	5	58.17	155.42	0.02062	0.0091114	Massive lava	R
AM16	23	6.13	317.7	0.01783	0.0107725	Massive lava	R
AM17 a	0.7			0.02071	0.0157	Massive lava	–
AM17 b				0.01932	0.0145556	Massive lava	–
AM18	4	47.73	140.81	0.02401	0.0155875	Massive lava	R
AM19	16	38.33	287.29	0.02284	0.0103571	Massive lava above the Neuquen sediments	–
AM20	6	39.03	78.03	0.01261	0.00752	Massive lava	–
AM21 a	0.3			0.01633	0.002555	Welded scoria	–
AM21 b				–	0.000885	Massive lava	–
AM22	2×10^{-2}			0.02039	–	Vesicular lava	–
AM23	2	53.64	94.79	0.02535	0.0137667	Massive lava	R
AM24 a	5×10^{-4}			0.00017	0.00026	Red clay, Neuquen sedimetary sequence	–
AM24 b	7×10^{-5}			–	0.0000835	Red clay	–
AM25	14	56.57	173.99	0.00357	0.0028889	Massive lava	R
AM26	5	46.2	72.15	0.00797	0.004906	Vesicular lava	R
AM27	19	–53.19	20.41	0.00984	0.0083325	Massive lava	N
AM28	9	28.44	210.5	0.01658	0.008285	Massive lava	R
AM29	21	23.33	7.98	0.02569	0.0089686	Massive lava	R

component was removed for all specimens at 10–20 mT, while the characteristic remanent magnetization direction was isolated in the 20–70 mT AF interval.

3.2 Aeromagnetic surveys

Regional aeromagnetic data were collected in 1968 by the Servicio Geológico Minero Argentino (Ferpozzi *et al.* 2007, Fig. 3a). The survey was flown at an altitude of about 2500 m a.s.l. forming a grid with N10° lines spaced 10 km apart and crossed by N100° lines spaced 30 km apart. Unfortunately this survey did not cover the Auca central edifice so it was only used to qualitatively characterize the longer wavelength magnetic features when the information in this and the high resolution survey discussed below were in agreement.

A high resolution aeromagnetic survey was conducted in the Auca and Señal Cerro Bayo areas by the Carson Aerogravity company in 2001 (Carson Aereogravity 2001). Magnetic data were collected using a Geometrics High Sensitivity Cesium Vapour Magnetometer at a sampling rate of 1 Hz. North–south and east–west lines were flown with 500 m spacing above the Auca summit crater and 2 km in the surrounding areas (Figs 3a and b). The nominal survey altitude was 2830 m above the mean sea level. A magnetic base station recording the diurnal variation was set up in the Rincon de los Sauces Airport. The data were corrected for diurnal variations using the base station, then the IGRF field was removed and finally the data were tie-line levelled to obtain the total magnetic intensity (TMI) anomaly (Fig. 3b).

4 MAGNETIC FIELD AND MODELLING

4.1 Magnetic field

The aim of magnetic surveying was to obtain information on the distribution of magnetic sources in this geological-tectonic setting to understand better how the volcano functioned, and also for the detection of oil traps hosted in volcanic structures and to interpret them in the framework of the geological knowledge of the area. We applied the MGinv3D (2013) inversion method (http://www.scicomap.com/MGinv3D.html) to the 2001 data set to model the volcano's magnetic properties and constrain the 3-D geological framework of Auca's inner structure. Comparing abrupt variations of susceptibility in the model with the magnetic properties of the known lithology and structures can be used to delineate lithological and/or structural discontinuities.

The Auca volcano magnetic anomaly field is characterized by features with a wide range of wavelengths. Local anomalies with wavelengths between 1.5 and 5 km are concentrated around the central crater (Fig. 3b). Regional anomalies with wavelengths between 40 and 80 km lie a few tens of kilometres outward from the central crater around the volcanic plateau. The similarity between regional anomalies and the anomalies recorded in the higher resolution 2001

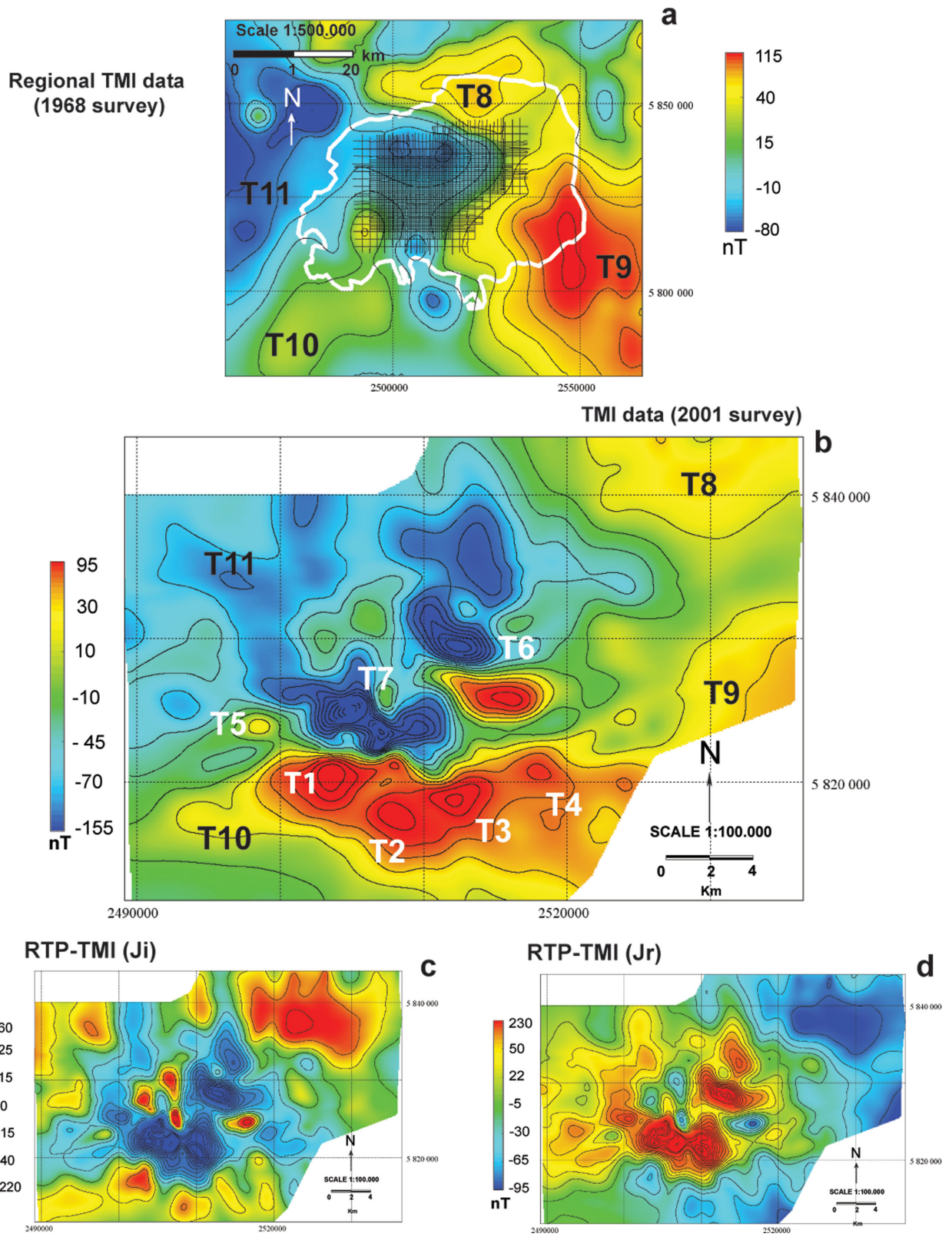

Figure 3. Auca magnetic anomaly fields: (a) 1968 regional TMI, black labels regional wavelengths (T9, T10 and T11), 2001 survey flight path in black lines, thicker white line indicates volcanic plateau border; (b) 2001 TMI data: local shorter wavelengths anomalies in white (T1, T2 T3, T4, T5, T6, T7 and T8), regional wavelengths anomalies in black (T9, T10 and T11); (c) Reduced-to-the-pole 2001 TMI data computed considering only the induction component Ji ($I = -38°$, $D = 3°$); (d) Reduced-to-the-pole 2001 TMI data computed with the remanence (Jr) acquired in a reverse field ($I = 38°$ and $D = 183°$).

survey is evident in Figs 3(a) and (b) (e.g. feature T9) The regional anomalies T8–T11 in Fig. 3(b) are not fully sampled in the 2001 survey and, therefore, their modelling is not possible with this data set. As mentioned above, the 1968 regional survey does not cover the Auca central crater area fully so it is only useful for providing a qualitative description of the longer wavelength features surrounding the 2001 survey. Regional magnetic anomalies surrounding the Auca volcanic plateau (white line in Fig. 3a) exhibit different signatures. The areas lying between the Añelo Basin, the Cerro Bayo volcanic structure and the region to the east of the Agrio fold and Thrust belt (Fig. 2), are characterized by magnetic lows (e.g. T11 in Figs 3a and b). This pattern is truncated to the south by a NE–SW to N–S striking positive feature related to the eastern flank of the Chihuidos structural high (T10). Positive high intensity magnetic anomalies occur east-southeast and north of the Auca plateau (T8 and T9).

4.2 Reduction-to-the-pole

The 2001 high resolution survey (black NS and EW lines in Fig. 3a and TMI field of Fig. 3b) covers the central part of the Auca volcano plateau outlined with the white border in Fig. 3(a). Foss & McKenzie (2009) categorize the exploration magnetic anomalies into three broad interpretational classes: simple, isolated anomalies from compact sources; complex anomalies from composite magnetic structures and magnetizations; and linear anomalies. On the basis of their classification scheme, two main groups of anomalies can be recognized in our area: (1) simple, compact dipolar anomalies lying in the Auca central plateau (T5–T7, Fig. 3b); (2) a string of coalesced anomalies on the southern flanks of the volcano (T1–T4, Fig. 3b) forming a 20 km long E–W elongated magnetic belt. While the identification of the (1) group anomalies is reasonably straightforward, the identification of the (2) group is more complex as they do not have a simple dipolar shape due to their spatial overlap and to the influence of the longer wavelength regional anomalies T9 and T10. The induced response of a discrete 3-D body in the current Earth's magnetic field ($I = -38^\circ$, $D = 3^\circ$) will exhibit a strong high to the north and a broader, smaller amplitude low to the south. Since the high-low pattern of individual dipolar features in the data is the opposite of that expected for a purely induced anomaly, the location and orientation of the dipoles suggest that the magnetization was mostly acquired during reversed polarity time periods of the Earth's magnetic field (e.g. Hinze *et al.* 2013). An exception is represented by the anomaly T7, whose negative lobe most likely lies to the south of the positive lobe, coalescing with the negative lobe of the T1 and T5 anomaly features. Thus, its source was probably emplaced during a period when the geomagnetic field was in the same direction as the Earth's current magnetic field.

The magnetic pattern discussed above attests to strong remanence of isolated and coalescing intrusive sources. This conclusion is confirmed by the measurements and analysis carried out on the lava flow samples collected in the field (Table 1) since about 2/3 of the volcanic rocks sampled show reverse magnetization, with the remainder having normal magnetization. Further, the Königsberger ratio is between 2.1 to about 200 with an average value of about 50. Therefore, the remanence component is the dominant component for most of the sampled lava flows. Due to the above described magnetic field characteristics, this result probably holds for all the magnetized rocks of the Auca volcano. Because of these normal and remanent magnetizations, the overall NRM of the sources, and their interference effects, are complex, one requires modelling approaches that can take the complexity into account as described in the next section.

Overcome the effects associated with the inclination of the field with latitude on the crustal magnetic anomaly field and facilitate its interpretation we carried out the reduced-to-the-pole (RTP) transformation. This filter aims to image the response of magnetic bodies that would be observed if the inducing were vertical (Baranov & Naudy 1964; Blakely 1995). This helps the interpretation of the magnetic anomaly field as it transforms the observed dipolar anomaly into a unipolar response located directly above its source (note that the unipolar response will be negative for a purely reversely magnetized source). The RTP algorithm assumes that both the ambient magnetic field and the rock magnetization have constant known directions (Blanco-Montenegro *et al.* 2006). Therefore, average angular values of the remanent and induced magnetization are required to perform effective RTP transformations. The Auca volcanic activity dates back to 2.03 ± 0.3 Ma to Pleistocene epoch, while the Payena retroarc volcanism and intrusions may be older. In this time frame, the Earth's magnetic field reversed six or seven times. Also, we have argued in the previous section that the TMI field of the volcano shows reversely magnetized sources. Therefore, their magnetization properties have to be considered in the RTP process. In the selection of values, we considered that a reverse polarity geomagnetic field was dominant during the Auca activity, or at least during the emplacement of most of the source bodies.

We selected the I and D values measured in our samples consistent with those found in literature for the study area (Laboratorio de Palaeomagnetismo 'Daniel Valencio'-Universidad de Buenos Aires, Propiedades magnéticas de los basaltos del area de Auca; unpublished data) because the sample orientation has an intrinsic error and this results in an uncertainty of about $\pm$ 10°–15° in I and D. To further restrict the range of the inclination values of the remanence, we selected the values consistent with the variation of inclination with the latitude for the geocentric axial dipole hypothesis. It is also well known that South America has remained in nearly the same position with respect to the geographical poles in the last 200 Myr (Besse & Courtillot 2002); this implies the lack of significant variations of the Earth's magnetic field inclination.

Therefore, we computed the RTP field with two separate transformations: (1) considering induced magnetization in the ambient field with $I = -38^\circ$ and $D = 3^\circ$ (Fig. 3c) and (2) assuming that all of the field was created by remanent magnetization acquired under the influence reverse polarity (remanent $I = 38^\circ$ and remanent $D = 183^\circ$), but observed in the present day ambient field (Fig. 3d, Blakely 1995).

The RTP calculated using the current Earth's field for both induced and remanent field directions displayed in Fig. 3(c) demonstrates that the RTP does not transform the TMI into an image showing only isolated positive and negative unipolar anomalies. This confirms the visual analysis of the TMI anomalies described above and shows that methods using only the current Earth's field direction will not be useful for modelling the Auca magnetic field. If we instead use the current Earth's field direction for the inducing half-transform of the RTP and the magnetization directions for the remanent half-transform, we obtain the transformed grid displayed in Fig. 3(d). This RTP transform has performed somewhat better in producing positive unipolar responses, which is consistent with the visual interpretation and rock measurements.

However the anomalies for T1, T2 and T6 show markedly dipolar responses with a low/blue to the south, so the RTP is clearly unable to simultaneously transform all anomalies to simple unipolar responses. The shapes of the anomalies in the RTP images in

Table 2. Magnetic and geometry characteristics of the bodies used for synthetic response calculations (Figs 4 and 5).

Name	Type	Width radius (m)	Depth Extent (m)	Susceptibility (SI)	Field *I*	Field *D*	Reverse magnetized
Body_A	Cylinder	1500	3000	0.25	38°	3°	Yes
Body_B	Cylinder	800	4600	0.375	38°	–45°	Yes
Body_C	Cylinder	1500	8700	0.125	38°	3°	Yes
Body_D	Cylinder	500	5400	0.5	38°	3°	Yes
Body_E	Prism	500 × 1200	200	0.25	–	–45°	No

Figs 3(c) and (d) demonstrate that while magnetic sources with reverse magnetizations are dominant in the area, there are significant areas of interference between responses from both induced and reversely remanently magnetized sources. This mix of magnetic responses necessitates the use a more sophisticated technique of inversion to properly model the distribution of sources. In fact, a simple inversion using only induced and normally and reversely magnetized remanent sources parallel to the direction of ambient induction will fail to correctly model some of the magnetic sources.

4.3 Modelling results

A number of techniques have been proposed to account for the effects of remanence in inversion modelling. One method is to transform the TMI data to calculate the total gradient or total amplitude response which is then modelled by inversion using a vertical magnetic field (Paine *et al.* 2001; Dransfield *et al.* 2003; Li *et al.* 2010). An alternative approach is to directly model the observed data by inverting it to determine both the magnetization intensity and direction (Shearer & Li 2004; Lelievre *et al.* 2006). The advantages of methods using a transformed response are that the transforms are simple to calculate and that standard 3-D magnetic inversion codes can be used to invert the resulting data.

Methods using the total gradient or total amplitude transforms of the observed TMI data are based on the observation that the transformed responses tend to be insensitive to the magnetization direction. As pointed out in Salem *et al.* (2002) and Li (2006), it can be shown that the total gradient of the TMI is independent of the direction of magnetization only for profiles across 2-D sources. There is nonetheless a much stronger spatial correlation between the highs in these transformed responses than there is in the original TMI and RTP data, so inversions using such data can potentially be useful in generating insight into the geometry of the magnetic sources despite the lack of theoretical rigour. These observations also apply to the VRMI transform, as described by Dransfield *et al.* (2003), in the context of using full vector magnetic measurements to deal with mixed induced and remanent magnetization in banded iron formations in the Hamersley Basin in the Western Australia. The VRMI is the magnitude A of the anomalous magnetic field response B, that is A = sqrt(Bx2+By2+Bz2). As vector data were not collected for the Auca 2001 aeromagnetic survey, the method of Lourenco & Morrison (1973) was used to derive the Bx, By and Bz components of the response from the TMI data using Fourier transforms and then to calculate the amplitude function A (i.e. VRMI).

In order to (1) evaluate the applicability of the VRMI in identifying regions of strong remanence with directions different to the main inducing field, and (2) verify the reliability of the subsequent inversion of the VRMI data, the simple cylindrical and tabular bodies detailed in Table 2 were defined with induced and remanent magnetization parameters chosen so that the synthetic responses qualitatively matched the amplitude and shapes of some of the main central features of the Auca TMI response. The location of these bodies is shown in Fig. 4(a) along with an image of the observed TMI data.

The total TMI response calculated for the synthetic model (i.e. the sum of remanent response and the response induced by the current ambient magnetic field) is displayed in Fig. 4(b). Fig. 4(c) shows the VRMI transform of the TMI response in Fig. 4(b) and was calculated using the ambient field direction for the Auca survey area ($I = -38°$, $D = 3°$). To determine how well the VRMI transform has performed in removing the effects of the different remanent and induced magnetization directions, Fig. 4(d) displays the response of the bodies calculated with vertical directions for both remanent and induced components. These latter two figures show that the VRMI transform performs well in reconstructing vertical field and magnetization response of the source bodies. The synthetic data (Figs 4b and c) were then modelled using the 3-D voxel inversion code MGinv3D (http://www.scicomap.com/MGinv3D.html) using a vertical magnetic field for both of them to reflect the fact that the anomalies in the VRMI image are effectively unipolar responses. The MGinv3D code uses the same approach as that described in Li & Oldenburg (2003) with the main differences being that the model volume is discretized using prismatic cells draped underneath the topography rather than simple rectangular prisms and that it uses the L-BFGS-B code of Zhu *et al.* (1994) to perform the smoothness constrained minimization of the data misfit.

We then carried out an unconstrained modelling of both the TMI and VRMI data using 250 m cubic cells with four padding cells at each edge and at the bottom of the mesh with a total mesh count of 193 (EW) by 135 (NS) and 25 (depth) covering a volume of 53 km × 39 km × 8.3 km. The TMI and VRMI grid was sampled at the mesh cell centres and the target misfit was set to be a constant 0.2 nT for the resulting 20 165 data points. Using unit smoothness weights in the *x*, *y* and *z* directions the target misfit was 0.2 nT and the achieved inversion misfit was 2.37 (using *z*-score data) and so the rms data misfit to the synthetic data is 0.5 nT.

The 0.05 SI susceptibility isosurface of the model generated by inverting the TMI response of the synthetic model for a vertical field is displayed as dark red in Fig. 5(a). It should be noted that although the 0.05 SI isosurface is significantly less than the susceptibilities of the source bodies detailed in Table 2, the smoothing inherent in the rms misfit based voxel inversions has made this isosurface the one that most clearly identifies the locations of the bodies. The inversion leads to some smearing of derived susceptibilities and the result is not the identical discrete susceptibilities. This is typical to all potential field imaging type inversions that do not artificially discretize the inversion result. Fig. 5(b) shows the same 0.05 isosurface level for the inversion of the VRMI transformed data in light purple. A comparison of these results shows that the inversion of the VRMI transformed data has distorted the shape of the source bodies and shifted the position of the smaller bodies slightly to the north, but overall the VRMI inversion has performed well in recovering the source bodies given that no assumptions were made on the magnetization direction.

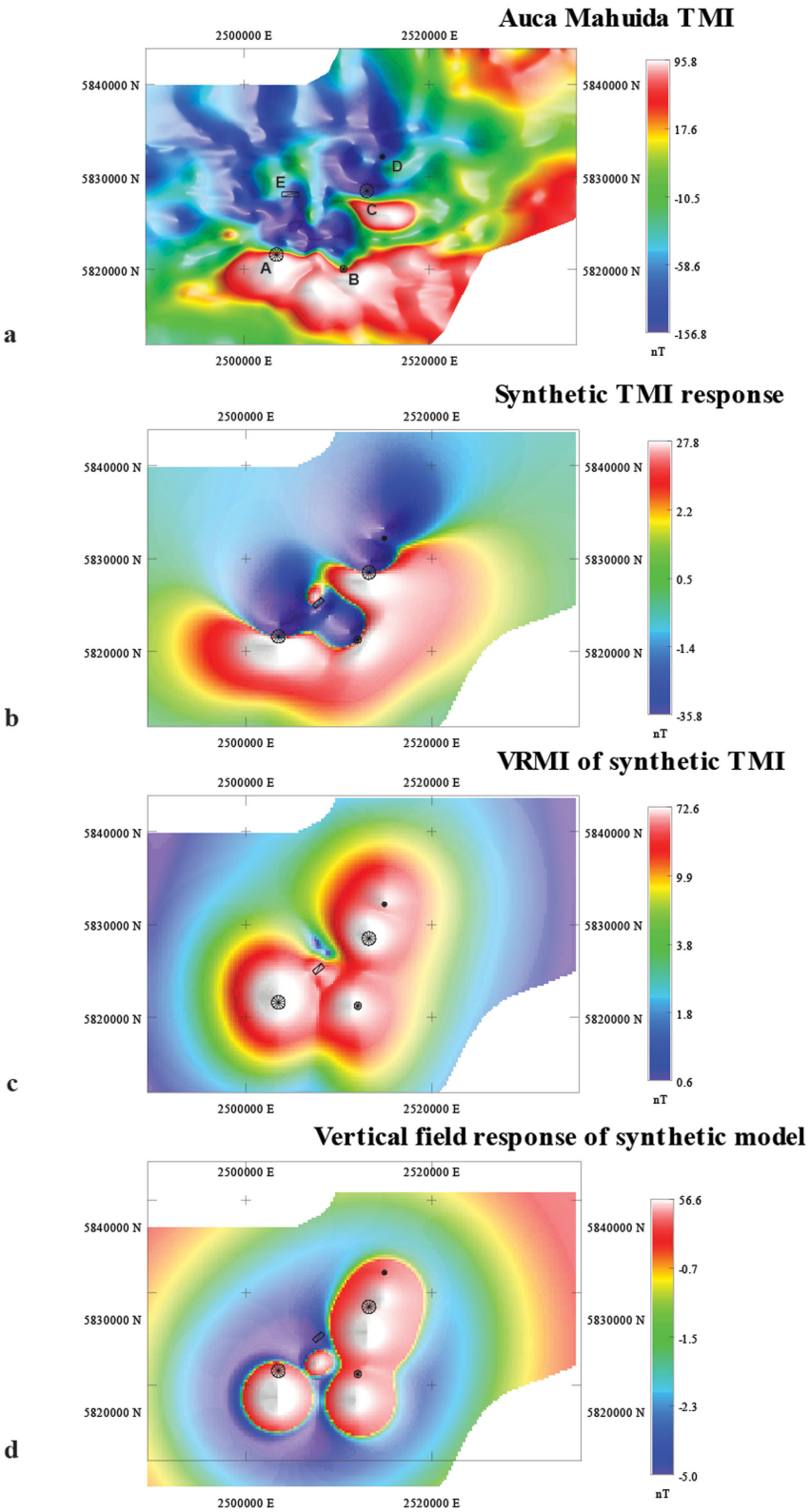

Figure 4. VRMI transformation tests on a simplistic synthetic model calculated for the same area of the Auca 2001 survey from five vertical magnetic cylinders. (a) 2001 TMI data with the location of synthetic bodies is shown with black circles; (b) synthetic TMI field computed using the current ambient magnetic field directions; (c) VRMI transformation of the synthetic TMI data and (d) vertical synthetic field response of the bodies.

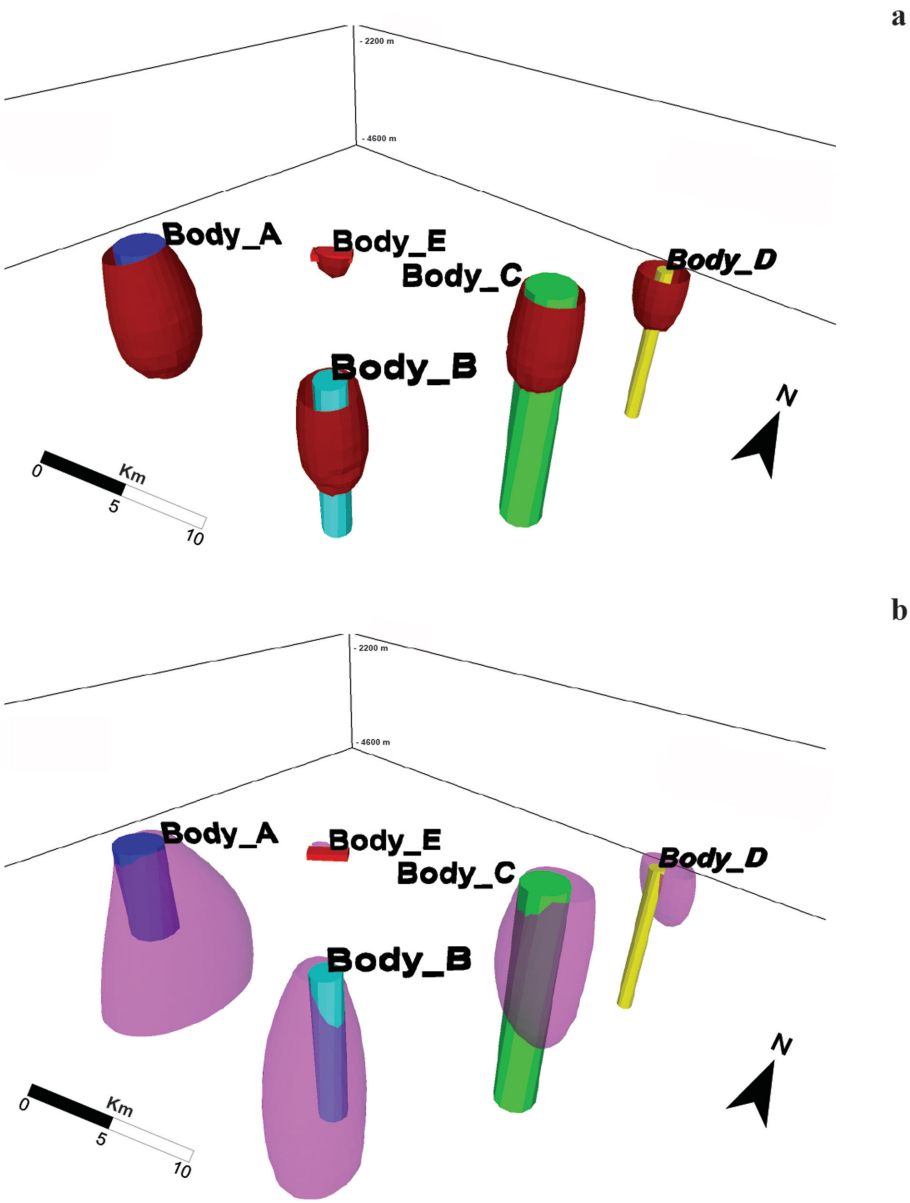

Figure 5. Perspective view of the 3-D voxel inversion results of the Fig. 4 model. (a) 0.05 SI inversion isosurface (red colour) generated from the vertical TMI; (b) 0.05 SI inversion isosurface (violet) generated from the VRMI transformation of the synthetic TMI data.

One of the biggest differences between real TMI responses and the transformed VRMI data is that the VRMI data tends to have more power at the low frequency end of the power spectrum than does the original TMI data. Therefore, if the VRMI data is simply treated as though it were the induced TMI response due to a vertical magnetic field, the model generated will have broader anomalous bodies with much larger depth extent than would be geologically reasonable. To counteract this effect it is usual to apply a residual filter to the VRMI data to attenuate the low frequency amplification in the data. For this study, we apply the FFT based mag layer extraction (MLE) filter (Jacobsen 1987; Cowan & Cowan 1993) with a layer thickness of 500 m to the VRMI (Fig. 6). This layer thickness was empirically chosen so that the slope of the power spectrum of the VRMI gave a reasonable match to that of the original TMI data.

On the basis of the above analysis, it appears that using the VRMI is likely to generate useful information about the subsurface distribution of magnetization at Auca and allow us to model the bodies generating the observed local anomaly of the central crater area. To do this we calculated the VRMI from the MLE 500 m residual of observed Auca TMI data using the current Earth's magnetic field direction as displayed in Fig. 6. We then used MGinv3D for an unconstrained modelling (without initial or reference model) of the VRMI data using 250 m cubic cells over the area of the 2001 survey with padding cells to expand the total volume to be 54 km E–W by 40 km N–S and 8.3 km in depth with a total mesh count of 185 (E–W) by 127 (N–S) and 21 (depth). The VRMI grid was sampled at the mesh cell centres and the target misfit was set to 0.25 nT for all of the 20 301 data points. Using unit smoothness weights in the x, y and z directions, the data were fit to rms data misfit of 0.6 nT after 300 iterations. The results of the inversion are shown in Figs 7(a), and (c) as 0.02 SI isosurface, while they are shown as colour levels and isoline of value 0.02 SI in Figs 7(b) and (d). The 0.020 SI isosurface of Fig. 7(a) was chosen to encompass

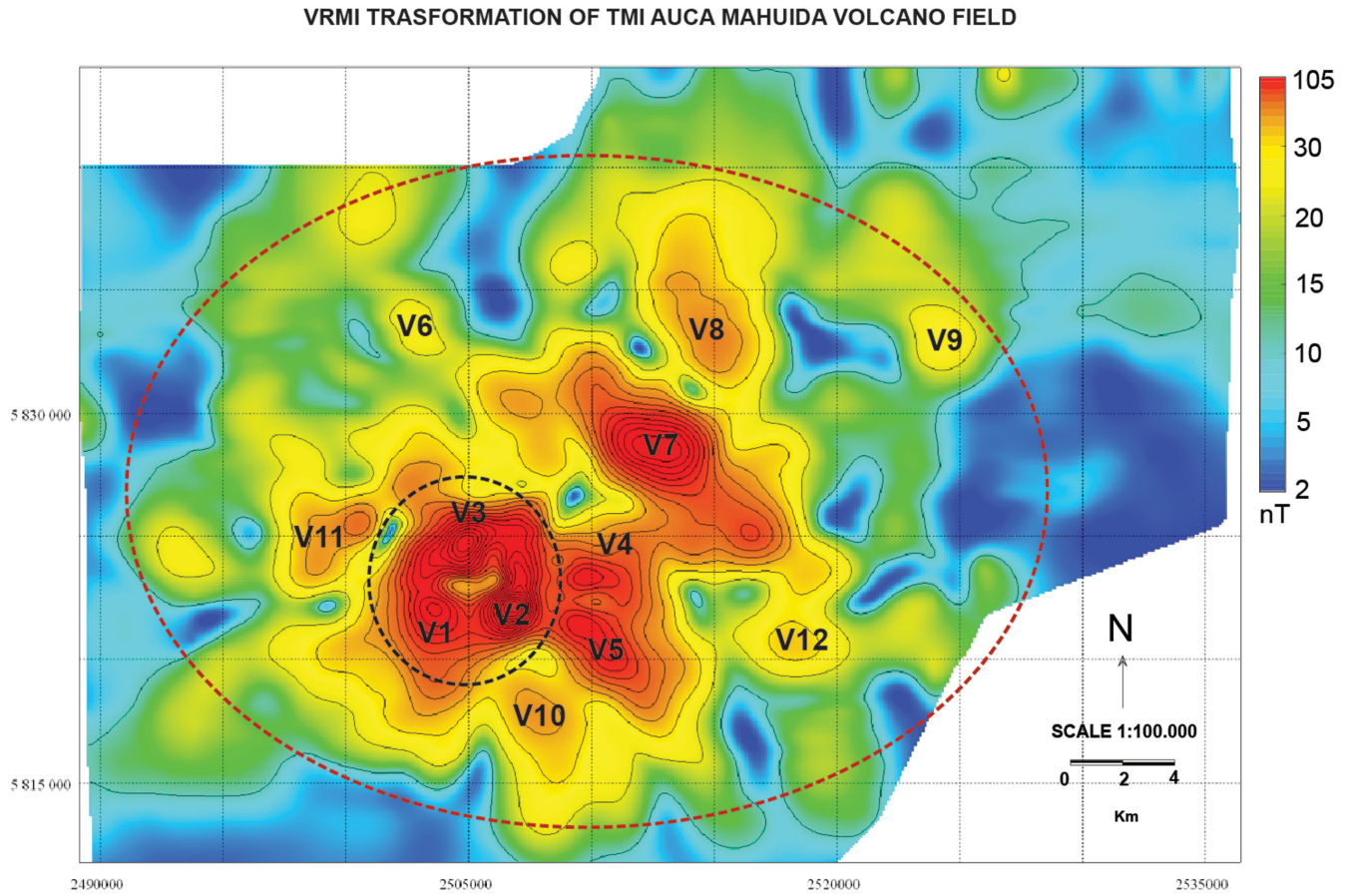

Figure 6. VRMI transformation of the observed 2001 TMI Auca data used in actual interpretation of the volcanic sources; black labels indicate the features discussed in the text (V1–V12). Red, dashed ellipse encloses the Auca VRMI anomalies. Black, thick dashed circle encloses the V1–V3 anomalies of the summit crater area.

most of the rock volume considered as having meaningful magnetic properties of the source bodies.

The criteria to evaluate the quality of the inversion are usually based on how closely the model agrees with the geo-structural framework of the area. Moreover, other misfit parameters may provide additional indications on the reliability of the obtained results. As an example, the differences between the observed and predicted data (Fig. 8), appears random except a slightly higher amplitude misfit in a few high amplitude VRMI field features. Therefore, the VRMI field is well resolved by the inversion model.

5 DISCUSSION

The magnetic anomalies in the Auca volcano (Fig. 3b) show different, partially superimposed sources, mainly magnetized in reverse epochs. Taking into account the 2.03–0.88 Ma age of the Auca eruptive activity, it appears likely that the volcanic activity mainly developed within the reversed polarity Matuyama Chron. The normal polarity anomalies most likely belong to the Olduvai and/or Jaramillo subchrons. The image of the RTP field calculated using both induced and remanent magnetization directions (Fig. 3d) shows that there are normal and reversely magnetized bodies in close proximity; this makes the anomalies difficult to interpret visually. For the same reason, inverse modelling of the TMI field will lead to results with limited interpretation capability in terms of source characteristics and the resolution of structural detail and, hence, we use the inversion of the VRMI transformed data (Fig. 6) as this is not significantly affected by different remanent directions. However, it is important to be aware that the potential field interpretation has an intrinsic limitation due to its no uniqueness; as a consequence, determination of actual structure beneath the Auca Mahuida volcano will require more constraints on depths and magnetizations than those presently available. In fact, in the region of inversion, we have only limited information from the VAM oil field, which covers a small portion of the modelling volume (Fig. 2). Moreover, our attempts to incorporate them suggested that the measured susceptibility values in the drill cores may not be representative of the bulk susceptibility of the sources inferred from the inversion.

As previously described, the properties of the samples shown in Table 1 indicate highly magnetized rocks with significant remanence. Most of these specimens were sampled in the central Auca edifice with an average total magnetization of 10 A/m. On the other hand, the highest susceptibility values from the inversion are about 0.14 SI, (Fig. 7d). These values correspond to a magnetization of 3 A m^{-1}, considering the Geomagnetic Reference Field of the survey date (IGRF2000) as induction field. To justify this difference, it is worth noting that the sampled massive lavas correspond to a part of the lava blanket extending up to 75 and 60 km in the E–W and N–S directions, respectively. These lavas are characterized by scoriaceous top and bottom portions, which would significantly lower the values of their bulk magnetization in samples (Table 1). Therefore, it is likely that the average magnetization of the Auca outcropping volcanic products is less than that measured in the lava

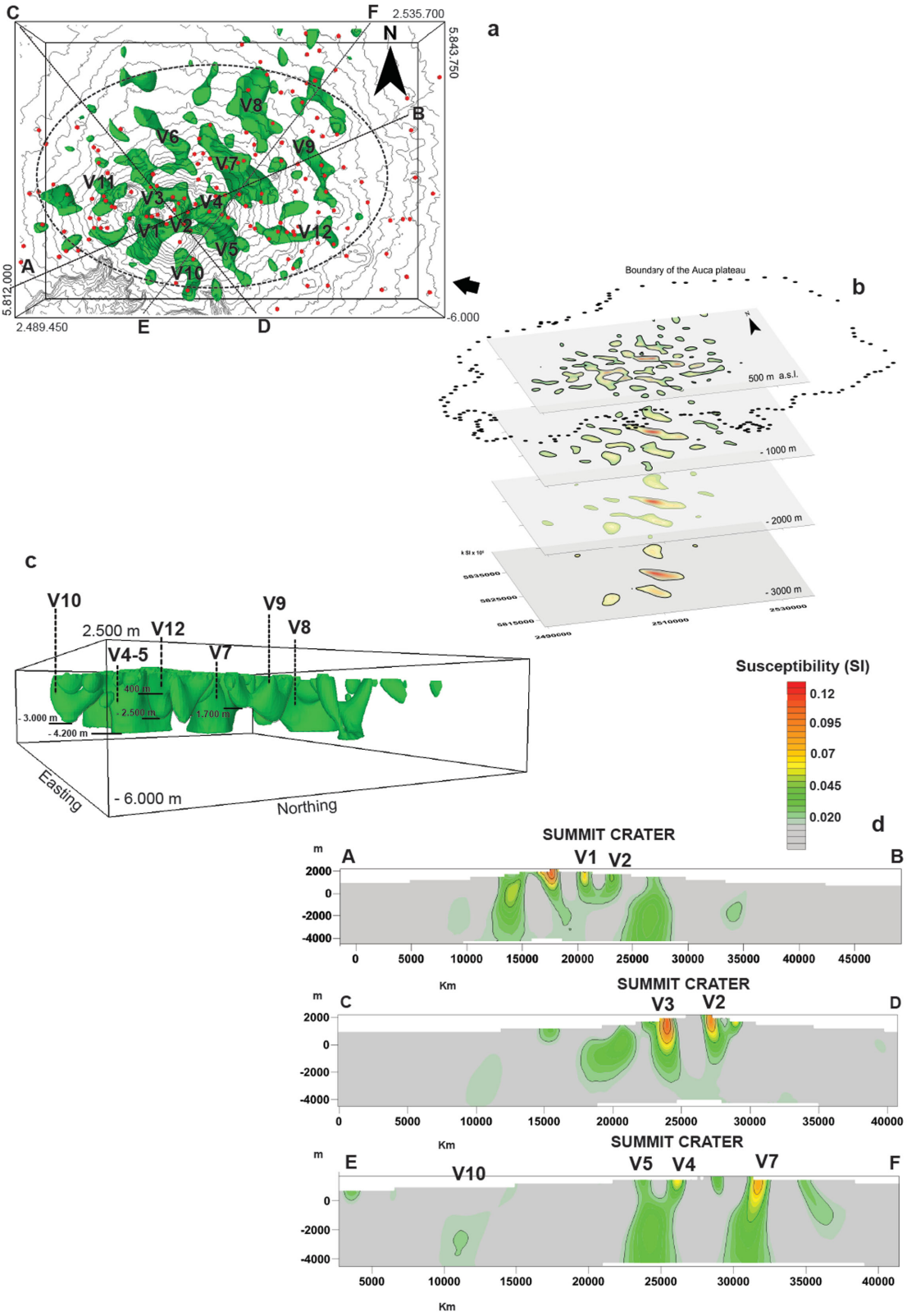

Figure 7. VRMI field inversion results showing 2-D and 3-D geometries of the magnetic field source bodies (through susceptibility isosurfaces and contours) and their depth extent. (a) Zenithal 3-D view of the 0.020 SI units isosurface together with the Digital Elevation Model contour lines and the locations of profiles (cross-sections) in Fig. 7(d). The black arrow at the bottom right of the figure represents the vantage point of Fig. 7(c), while the red dots are the volcanic cones; (b) 2-D depth slices of the VRMI inversion solutions (susceptibilities ≥0.02 SI, contoured by a black line); the colour scale (for panels b and d) is also shown to the right; (c) a lateral view (southeastern) of the main sources and their depth extent (labelled); (d) depth sections along profiles AB, CD and EF (from Fig. 7a), with susceptibility contours ≥ 0.020 SI.

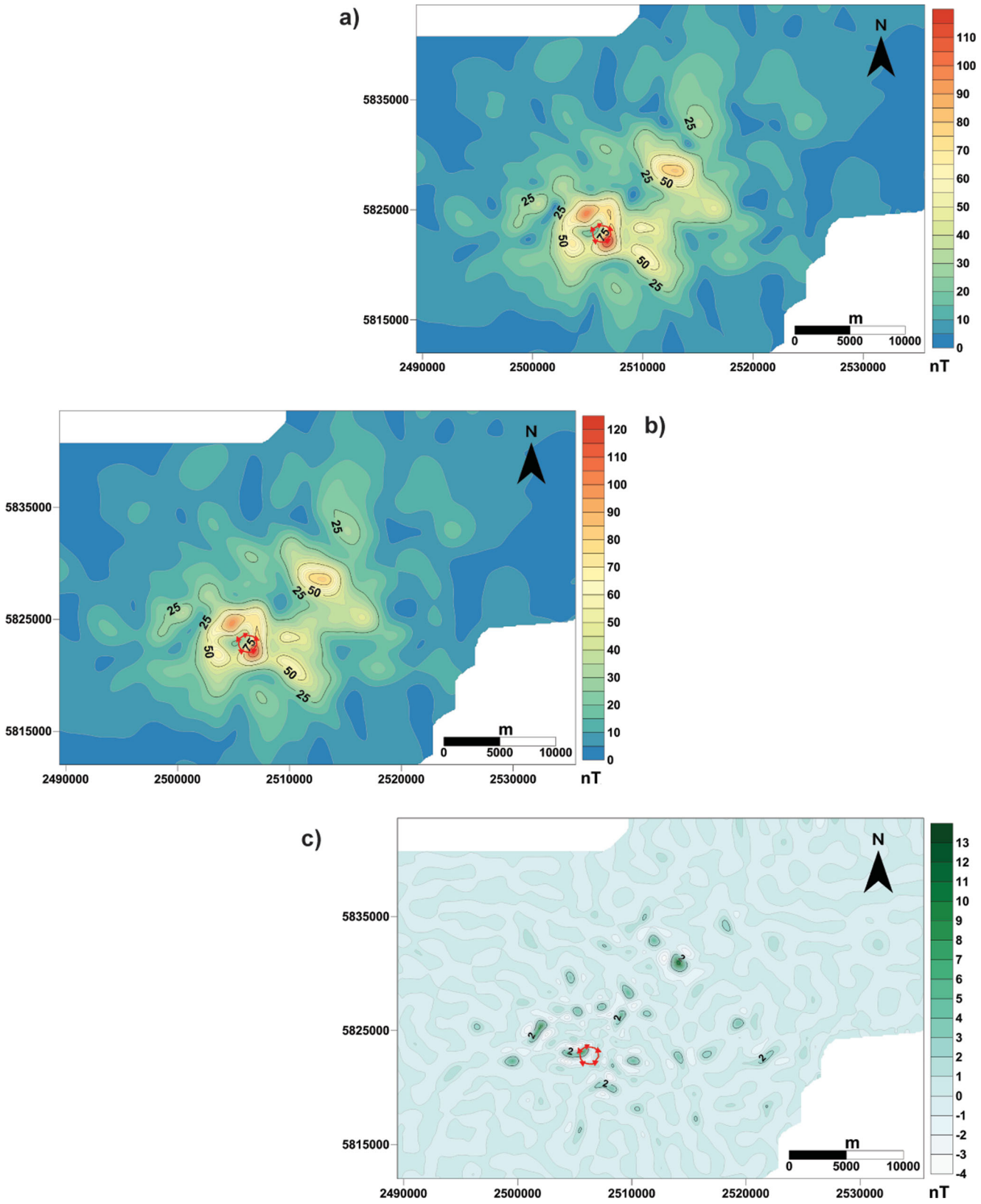

Figure 8. Inversion errors. (a) Vector residual magnetic intensity (VRMI) obtained from real TMI data; (b) Modelled Vector Residual Magnetic Intensity (VRMI); (c) Difference between the maps in (a) and (b). The red circle represents the position of the Auca Mahuida summit crater.

samples. Moreover, the filtering process of TMI data described in the previous section determined an attenuation of the low frequency content; as a consequence, the total magnetization of the source body obtained inverting the VRMI field was lowered. In addition, the inversion technique we adopted generates smooth models that smear the sources and hence lower the peak susceptibilities.

The VRMI field has more interpretive detail than the TMI or RTP fields in this example with sources of different remanent magnetization. The VRMI field highs depict a slightly E–W elongated feature (red dashed ellipse in Fig. 6). The central crater area is characterized by a complex VRMI pattern with higher values of the field forming a ring-like magnetic structure centred on the Auca summit crater (anomalies V1, V2 and V3 inside the black dashed circle in Fig. 6). In the eastern sector of the volcano, the higher intensity anomalies V4, V5, V7 are NW–SE elongated. The V6 and V8 lower intensity highs are aligned NW–SE. A NNW–SSE fault system may also exist (Fig. 1) along the trend from V12 to V8. This general preferred strike is that of the 'Entre Lomas' fault system, which mainly affects the Auca eastern sector (Fig. 1c) and that of the axis of the antiform affecting the Neuquén basin sediments below the volcano. The subcircular V9 anomaly overlies the larger cone (diameter up to 3 km) of the Auca plateau.

The results of the inversion (Fig. 7a) identify numerous sources located within an E–W elongated area (red and black dashed ellipses of Fig. 6 and Fig. 7a), which roughly corresponds to the Auca central edifice. Numerous NW–SE elongated bodies and less extensive E–W elongated bodies are concentrated in the central and eastern sectors of the volcano (Fig. 7a); the more extended of these bodies correspond to the anomalies V4–V5, V7 and V8 in the VRMI map (Fig. 6). A subcircular, ring-like body is located below the summit crater area; this body represents the source of the V1, V2 and V3 anomalies (Figs 7a, b and d). Smaller, subspherical to ellipsoidal bodies also occur, mainly in the periphery of the Auca plateau.

The depths of the bodies recognized from the magnetic modelling below the Auca volcano ranges between 400 m a.s.l. to 4 km below the sea level (Figs 7c and d). The deeper bodies are those that are NW–SE elongated and the subcircular one located to the east and northeast of the central crater. Some of these bodies enlarge at depths larger than 1300–1500 m (V4, V5 and V7, Figs 7a and c), where, according to deep well data, the thickness of the basaltic intrusions, which is 50–100 m at 1300 m depth, also significantly increases to 200–400 m at depth larger than 1300 m. The geometries of the elongated bodies are consistent with those of coalescing dikes and laccoliths. The deeper, larger bodies located in the central sector of the volcano overlap the zone of maximum vent density (Ventura *et al.* 2012). The subcircular source located below the summit crater could represent an annular intrusive body (Fig. 7a). This interpretation is supported by boreholes placed close to the crater area (Fig. 1b, e.g. VAM x-1), which highlight the presence of intrusives up to 100-m-thick concentrated below the Centenario Formation at depth between 900 and 1800 m below the topographic surface. The larger scale NW–SE elongated source bodies located in the Auca central and eastern sectors suggest the presence of dike- to laccolith-like bodies, possibly reflecting intrusions along the NW–SE striking faults of the 'Entre Lomas' fault system, which also affects the basement below the Auca eastern sector (V7, V4 and V5, Figs 6 and 7a). The elongated sources located at the periphery of the investigated area may represent the crystallized, shallow plumbing systems of the isolated cones of the plateau lying at lower altitude with respect to the central edifice (V9 and V12, Fig. 7a).

The above magnetic sources likely reflect the intrusives of the Auca feeding system. The intrusions produced vertical displacement (uplift) and faulting of the sediments and formed structural highs that, in some cases, became hydrocarbon traps. This mechanism generated productive hydrocarbon accumulations located on the northern foothills of the volcanic shield, about 3 km north from the central crater (YPF internal report). The volcanic activity also affected the hydrocarbon reservoirs in at least two more ways, namely the possible enhancement of reservoir properties through thermally induced fractures, and the charging of the igneous bodies themselves with oil, also inside fractures and pores (YPF internal report). Thus, knowledge of the distribution and morphology of the intrusive bodies will be helpful in evaluating prospective petroleum traps in the oil field, as well as improving the characterization of the oil and gas reservoirs (e.g. the existence of different reservoir compartments as a result of faulting or traps related to intrusives).

Analysis of the magnetic anomaly field furnished useful information about the plumbing system and position and geometries of intrusions, which have affected the petroleum system. Because of the trends of magnetic anomalies corresponding to some of the structural elements in the region, the intrusion of igneous bodies is thought to have occurred along previously existing faults, leading to the formation of laccoliths or sills. These bodies must have thermally contributed to hydrocarbon generation and maturation in the source rock. Besides, the igneous intrusions themselves are believed to have altered the structure of the pre-existing sedimentary layers to help control the formation of reservoirs and traps.

6 CONCLUSIONS

The overall E–W elongation of the Auca area enclosing the magnetic sources and the outcropping vents indicates a deeper structure along which mantle intrusions rose to the upper crust. In the Auca area, this deep structure is the Cortaderas lineament, which represents the southern boundary of the shallower Miocene subduction. The orientation of the maximum horizontal stress in the Neuquén Basin and Auca area is E–W by the model of Nakamura (1977), the line of volcanoes and their plumbing system follows the orientation of the maximum horizontal stress. The results of geomorphological analysis carried out by Ventura *et al.* (2012) suggest that the geometry of Auca's deeper plumbing system is mainly controlled by the E–W Andean compression and consequent N–S extension. On the basis of our observations and modelling, the shallower feeding system is controlled by the more superficial NW–SE striking tectonic structures of the 'Entre Lomas' fault system. This latter would imply that the faulting in the region was followed by the magma intruded along the zones of weaknesses.

Our results also indicate that the Auca central sector below the summit crater is characterized by coalescing magnetic (intrusive) bodies forming an annular structure. This local feature suggests the occurrence of radial extension possibly due to magma pressure in the confined crater area. Therefore, Auca's shallow plumbing system(s) appears to be controlled by magma pressure at a local scale, whereas pre-existing regional tectonic structures represent the main magma pathways.

As stated previously, the petroleum systems (source and reservoir rocks) in the Auca area have been affected by igneous intrusions (Rossello *et al.* 2002). Therefore, the magnetic sources underlying the volcano, which represent subvolcanic and intrusive bodies, may contain hydrocarbons. The results of our analysis suggests that it may be possible to find reservoirs in the upper part of the central volcano. In fact, boreholes pumping oil from intrusions are located in the southern flank of the central crater, less than 100 m from the

crater rim, closer to the locations of annular source bodies (V1–V2). The interpreted magnetic bodies lie mainly along the NW–SE striking faults system, which, in turn, may have played a role in the migration of the hydrocarbons from the source rocks (the Vaca Muerta shales, Fig. 1b) to the oil traps (sedimentary rocks and intrusive bodies).

The results of our study show how magnetic data can be used to (1) constrain the geometry of the shallow plumbing system of volcanic complexes, (2) investigate the influence of tectonics on the subsurface structure of volcanoes and (3) obtain information on the depth and geometry of oil reservoirs and/or traps located in volcanic areas. The analytical approach used here could be extended to other tectonic structures and oil systems stored in rocks with remanent magnetic sources.

ACKNOWLEDGEMENTS

We thank the YPF colleagues at Rincón de Los Sauces for the assistance in the field and numerous discussions. This study was carried out with INGV funds within an INGV-YPF scientific agreement. The used data are the property of YPF s.a. and any request for them should be directed to YPF s.a. (laura.longo@ypf.com).

REFERENCES

Alberdi-Genolet, M., Cavallaro, A., Hernandez, N., Crosta, D.E. & Martinez, L., 2013. Magmatic events and sour crude oils in the Malargüe area of the Neuquén Basin, Argentina, *Mar. Pet. Geol.,* **43,** 48–62.

Baranov, V. & Naudy, H., 1964. Numerical calculation of the formula of reduction to the magnetic pole, *Geophysics,* **29,** 67–79.

Barberi, F., Gandino, A., Gioncada, A., La Torre, P., Sbrana, A. & Zenucchini, C., 1994. The deep structure of the Eolian arc (Filicudi-Panarea-Vulcano sector) in light of gravity, magnetic and volcanological data, *J. Volc. geotherm. Res.,* **61,** 189–206.

Bermudez, A. & Delpino, D., 1998. Estudio de testigos corona de rocas igneas intrusivas reservorios de hidrocarburos y de las secuencias extrusivas del volcan Auca Mahuida, YPF internal report, Buenos Aires, 132 pp.

Besse, J. & Courtillot, V., 2002. Apparent and true polar wander and the geometry of the geomagnetic field over the last 200 Myr., *J. geophys. Res.,* **107**(B11), 2300, doi:10.1029/2000jb000050.

Blakely, R.J., 1995. *Potential Theory in Gravity and Magnetic Applications*, University Press, 441 pp.

Blanco-Montenegro, I., De Ritis, R. & Chiappini, M., 2006. Imaging and modelling the subsurface structure of volcanic calderas with high-resolution aeromagnetic data at Vulcano (Aeolian islands, Italy), *BUL. Volcanol.,* **69**(6), 643–659.

Caratori Tontini, F., Cocchi, L., Muccini, F., Carmisciano, C., Marani, M., Bonatti, E., Ligi, M. & Boschi, E., 2010. Potential-field modeling of collapse-prone submarine volcanoes in the southern Tyrrhenian Sea (Italy), *Geophys. Res. Lett.,* **37,** L03305, doi:10.1029/2009GL041757.

Carson Aereogravity. Volcán Auca Mahuida and Señal Cerro Bayo Exploration Lots (March 28, 2001 - June 10, 2001) For YPF S.A., Argentina Data Processing Report, 2001.

Cowan, D.R. & Cowan, S., 1993. Separation filtering applied to aeromagnetic data, *Explor. Geophys.,* **24,** 429–436.

Cristallini, E.O., Bottesi, G., Gavarrino, A., Rodriguez, L., Tomezzoli, R. & Comeron, R., 2006. Synrift geometry of the Neuquén Basin in the northeastern Neuquén Province, Argentina, in *Evolution of the Andean Margin: A Tectonic and Magmatic View from the Andes to the Neuquén Basin (35°–39° Latitude),* Vol. 407, pp. 147–161, eds En Kay, S.M. & Ramos, V.A., Geol. Soc. Am.

De Ritis, R., Ventura, G & Chiappini, M., 2007. Aeromagnetic anomalies reveal hidden tectonic and volcanic structures in the central sector of the Aeolian Islands, Southern Tyrrhenian Sea, Italy, *J. geophys. Res.,* **112**, doi:10.1029/2006JB004639.

De Ritis, R., Ventura, G., Chiappini, M., Carluccio, R. & Von Frese, R., 2010. Regional magnetic and gravity anomaly correlations of the Southern Tyrrhenian Sea, *Phys. Earth planet. Inter.,* **181**(1–2), 27–41.

De Ritis, R., Ravat, D., Ventura, G. & Chiappini, M., 2013. Curie isotherm depth from aeromagnetic data constraining shallow heat source depths in the central Aeolian Ridge (Southern Tyrrhenian Sea, Italy), *Bull. Volcanol.,* **75,** doi:10.1007/s00445-013-0710-9.

Dransfield, M., Christensen, A. & Liu, G., 2003. Airborne vector magnetics mapping of remanently magnetized banded iron formations at Rocklea, Western Australia, *Explor. Geophys.,* **34,** 93–96.

Ferpozzi, F., Peñalva, G. & Vargas, D., 2007. Bloque Cuenca Neuquina 1968; Levantamiento aeromagnético analógico: digitalización, reprocesamiento y edición, Report, Servicio Geológico Minero Argentino.

Finn, C., Sisson, T.W. & Deszcz-Pan, M., 2001. Aerogeophysical measurements of collapse-phrone hydrothermally altered zones at Mount Rainer volcano, *Nature,* **409,** 600–603.

Foss, C. & McKenzie, K.B., 2009. Strategies to model a suite of remanent magnetization anomalies: an example from the Georgetown area of Queensland, in Proceedings of the ASEG Extended Abstracts Adelaide.

Gudnason, J., Holm, P.M., Søager, N. & Llambías, E.J., 2012. Geochronology of the late Pliocene to recent volcanic activity in the Payenia back-arc volcanic province, Mendoza Argentina, *J. S. Am. Earth. Sci.,* **37,** 191–201.

Guzman, C., Cristallini, E. & Bottesi, G., 2007. Contemporary stress orientations in the Andean retroarc between 34°S and 39°S from borehole breakout analysis, *Tectonics,* **26,** TC3016, doi:10.1029/2006TC001958.

Guzman, C.G. & Cristallini, E.O., 2009. Contemporary stress orientations from borehole breakout analysis in the southernmost flat-slab boundary Andean retroarc (32.4° and 33.4°S), *J. geophys. Res.,* **114,** B02406, doi:10.1029/2007JB005505.

Hinze, W.J., Von Frese, R.R.B. & Saad, A.H., 2013. *Gravity and Magnetic Exploration,* Cambridge Univ. Press, pp. 525.

Jacobsen, B.H., 1987. A case for upward continuation as a standard separation filter for potential-field maps, *Geophysics,* **52,** 1138–1148.

Kay, S.M. & Ramos, V.A., 2006. Evolution of an Andean Margin: a tectonic and magmatic view from the Andes to the Neuquén Basin (35–39°S), *Geol. S. Am. S.,* **407,** 19–60.

Kay, S.M., Burns, M. & Copeland, P., 2006. Upper Cretaceous to Holocene magmatism and evidence for transient Miocene shallowing of the Andean subduction zone under the northern Neuquén Basin, *Geol. Soc. Am. Mem.,* **407,** 19–60.

Kay, S.M., Helen Jones, A. & Kay, R.W., 2013. Origin of tertiary to recent EM- and subduction-like chemical and isotopic signatures in Auca Mahuida Region (37° to 38°S) and other Patagonian Plateau Lavas, *Contrib. Mineral. Petrol.,* **166,** 165–192.

Khazaradze, G. & Klotz, J., 2003. Short- and long-term effects of GPS measured crustal deformation rates along the south-central Andes, *J. geophys. Res.,* **108**(B6), 2289, doi:10.1029/2002JB001879.

Kirschvink, J.L., 1980. The least-squares line and plane and the analysis of paleomagnetic data, *Geophys., J. R. astron. Soc.,* **62,** 699–718.

Lelievre, P.G., Oldenburg, D.W. & Phillips, N., 2006. 3D magnetic inversion for total magnetization in areas with complicated remanence, in *Proceedings of SEG Annual Meeting,* New Orleans.

Li, X., 2006. Understanding 3D analytic signal amplitude, *Geophysics,* **71**(2), L13–L16.

Li, Y. & Oldenburg, D.W., 2003. Fast inversion of large-scale magnetic data using wavelet transforms and a logarithmic barrier method, *Geophys. J. Int.,* **152,** 251–265.

Li, Y., Shearer, S.E., Haney, M.M. & Dannemiller, N., 2010. Comprehensive approaches to 3D inversion of magnetic data affected by remanent magnetization, *Geophysics,* **75**(1), L1–L11.

Liu, J., Wang, P., Zhang, Y., Bian, W., Huang, Y., Tang, H. & Chen, X., 2012. Volcanic rock-hosted natural hydrocarbon resources: a review, in *Updates in Volcanology - New Advances in Understanding Volcanic Systems*, ed. Nemeth, K., InTech, doi:10.5772/54587.

Available at: http://www.intechopen.com/books/updates-in-volcanology-new-advances-in-understanding-volcanic-systems/volcanic-rock-hosted-natural-hydrocarbon-resources-a-review.

Lourenco, J.S. & Morrison, H.F., 1973. Vector magnetic anomalies derived from measurements of a single component of the field, *Geophysics,* **38,** 359–368.

Mazzarini, F., Fornaciai, A., Bistacchi, A. & Pasquare, F.A., 2008. Fissural volcanism, polygenetic volcanic fields, and crustal thickness in the Payen Volcanic Complex on the central Andes foreland (Mendoza, Argentina), *Geochem. Geophys. Geosyst.,* **9,** Q09002, doi:10.1029/2008GC002037.

Messager, G., Nivière, B., Martinod, J., Lacan, P. & Xavier, J.P., 2010. Geomorphic evidence for Plio Quaternary compression in the Andean foothills of the southern Neuquén Basin, Argentina, *Tectonics,* **29,** TC4003, doi:10.1029/2009TC002609.

MGinv3D 1.24, November 2013. Scientific Computing and Applications, Available at: http://www.scicomap.com/MGinv3D.htm.

Nakamura, K., 1977. Volcanoes as possible indicators of tectonic stress orientation—principle and proposal, *J. Volc. Geotherm. Res.,* **2,** 1–16.

Nicolosi, I., D'Ajello Caracciolo, F., Branca, S., Ventura, G. & Chiappini, M., 2014. Volcanic conduit migration over a basement landslide at Mount Etna (Italy), *Scientific Reports,* **4,** 5293, doi:10.1038/srep05293.

Paine, J., Haederle, M. & Flis, M., 2001. Using transformed TMI data to invert for remanently magnetized bodies, *Explor. Geophys.,* **32,** 238–242.

Phillips, J.D., 2004. Can we estimate total magnetization directions from aeromagnetic data using Helbig's integrals?, *Earth Planets Space,* **57,** 681–689.

Portniaguine, O. & Zhdanov, M.S., 2002. 3-D magnetic inversion with data compression and image focusing, *Geophysics,* **67,** 1532–1541.

Ramos, V.A. & Folguera, A., 2010. Payenia volcanic province in the Southern Andes: an appraisal of an exceptional Quaternary tectonic setting, *J. Volc. Geotherm. Res.,* **201,** 53–64.

Ramos, V.A. & Kay, S.M., 2006. Overview over the tectonic evolution of the southern Central Andes of Mendoza and Neuquén (35°–39° S latitude), in *Evolution of an Andean Margin: a Tectonic and Magmatic View from the Andes to the Neuquén Basin (35°–39° S latitude),* Vol. 407, pp. 1–18, eds Kay, S.M. & Ramos, V.A., Geological Society of America, Special Paper.

Rodriguez Monreal, F., Villar, H.J., Baudino, R., Delpino, D. & Zencich, S., 2009. Modeling an atypical petroleum system: a case study of hydrocarbon generation, migration and accumulation related to igneous intrusions in the Neuquen Basin, Argentina, *Mar. Petrol. Geol.,* **26,** 590–605.

Rollin, P.J., Cassidy, J., Locke, C.A. & Rymer, H., 2000. Evolution of the magmatic plumbing system at Mt Etna: new evidence from gravity and magnetic data, *Terra Nova,* **12,** 193–198.

Rossello, E.A., Cobbold, P.R., Diraison, M. & Arnaud, N., 2002. Auca Mahuida (Neuquén basin, Argentina): a Quaternary shield volcano on a hydrocarbon-producing substrate, in *Proceedings of the 6th International Symposium on Andean Geodynamics (ISAG 2002)*, Extended Abstracts, Barcelona, Univ. de Barcelona: Instituto Geologico y Minero de España, pp. 549–552.

Salem, A., Ravat, D., Gamey, T.J. & Ushijima, K., 2002. Analytic signal approach and its applicability in environmental magnetic investigations, *J. appl. Geophys.,* **49,** 231–244.

Shearer, S. & Li, Y., 2004. 3D Inversion of magnetic total gradient data in the presence of remanent magnetization, *SEG Technical Program Expanded Abstracts*, pp. 774–777.

Ventura, G., De Ritis, R., Longo, M. & Chiappini, M., 2012. Terrain characterization and structural control of the Auca Mahuida volcanism (Neuquén Basin, Argentina), *Int. J. Geogr. Inf. Sci.,* **27,** 1469–1480.

Zapata, T. & Folguera, A., 2005. Tectonic evolution of the Andean fold and thrust belt of the Southern Neuquén basin, Argentina. in *The Neuquén Basin, A Case Study in Sequence Stratigraphy and Basin Dynamics,* Vol. 252, pp. 37–56, eds Veiga, G., Spalletti, L., Howell, J. & Schwarz, E., Geol. Soc. Lond. Special Publication.

Zhu, C., Byrd, R.H., Lu, P. & Nocedal, J., 1994. L-BFGS-B: a limited memory FORTRAN code for solving bound constrained optimization problems', *Tech. Report,* NAM-11, EECS Department, Northwestern University.

Zijderveld, J.D.A., 1967. A.C. demagnetization of rocks: analysis of results, in *Methods in Palaeomagnetism*, pp. 254–286, eds Collinson, D.W., Creer, K.M. & Runcorn, S.K., Elsevier.